AIP | Applied Physics Letters

A geometry for optimizing nanoscale magnetic resonance force microscopy

Fei Xue, P. Peddibhotla, M. Montinaro, D. P. Weber, and M. Poggio

Citation: Applied Physics Letters **98**, 163103 (2011); doi: 10.1063/1.3579521
View online: http://dx.doi.org/10.1063/1.3579521
View Table of Contents: http://scitation.aip.org/content/aip/journal/apl/98/16?ver=pdfcov
Published by the AIP Publishing

A geometry for optimizing nanoscale magnetic resonance force microscopy

Fei Xue (薛 飞), P. Peddibhotla, M. Montinaro, D. P. Weber, and M. Poggio[a)]
Department of Physics, University of Basel, Klingelbergstrasse 82, 4056 Basel, Switzerland

(Received 2 February 2011; accepted 19 March 2011; published online 18 April 2011)

We implement magnetic resonance force microscopy (MRFM) in an experimental geometry, where the long axis of the cantilever is normal to both the external magnetic field and the rf microwire source. Measurements are made of the statistical polarization of ^{1}H in polystyrene with negligible magnetic dissipation, gradients greater than 10^5 T/m within 100 nm of the magnetic tip, and rotating rf magnetic fields over 12 mT at 115 MHz. This geometry could facilitate the application of nanometer-scale MRFM to nuclear species with low gyromagnetic ratios and samples with broadened resonances, such as In spins in quantum dots. © *2011 American Institute of Physics*. [doi:10.1063/1.3579521]

In the past several years, researchers have employed force-detected nuclear magnetic resonance to extend the resolution of magnetic resonance imaging (MRI) into the nanometer scale.[1] In 2009, using a technique known as magnetic resonance force microscopy (MRFM), researchers made three-dimensional images of individual tobacco mosaic viruses with a resolution better than 10 nm.[2] The sensitivity of MRFM now surpasses the sensitivity of conventional, inductively detected magnetic resonance by eight orders of magnitude, allowing for the detection of small spin ensembles containing less than 10^4 nuclear moments. This increased sensitivity has opened the door for MRI of structures that, until now, had been inaccessible to conventional techniques, e.g., individual virus particles, thin films,[3] and—potentially—quantum dots (QDs).

The most recent implementations achieving the highest sensitivity[2,3] have utilized a sample-on-cantilever configuration with the sample affixed to the end of an ultrasensitive Si cantilever having a spring constant typically on the order of 100 μN/m. The sample is positioned within 100 nm of a FeCo magnetic tip in a "pendulum" geometry so as to avoid snap in to contact.[6] The magnetic tip is patterned on top of an rf microwire, which acts as an rf magnetic field source.

One important limitation to the spin sensitivity is mechanical dissipation experienced by the cantilever in a static magnetic field. As MRFM experiments are carried out at elevated magnetic fields in order to saturate the magnetic tips, magnetic dissipation in the cantilever oscillator can significantly reduce the spin sensitivity of a measurement. For mechanical oscillators containing magnetic materials, dissipation that depends on magnetic field is expected and has been observed.[7,8] Magnetic dissipation should not affect oscillators containing no magnetic material. Recently, however, it has been reported that the application of a magnetic field can cause significant mechanical dissipation in micromechanical oscillators made of nominally nonmagnetic Si.[7,9–11] As shown in Fig. 1, this kind of dissipation has also been observed as a loss in mechanical quality factor Q in some bare ultrasensitive Si cantilevers used for recent MRFM. Its origin is likely the unintentional presence of impurities or defects with magnetic anisotropy, probably introduced during processing.

One way to eliminate this type of dissipation without having to eliminate the presence of magnetic impurities is to ensure that as the cantilever oscillates, it does not change its angle with respect to the applied magnetic field $\mathbf{B}_0 = B_0\hat{z}$, as seen in Fig. 1. We therefore show MRFM measurements of the statistical polarization of ^{1}H in a polystyrene particle, where we apply $\mathbf{B}_0$ along the cantilever's angular rotation vector. As shown in Fig. 2, the force detection apparatus is similar to the apparatus described in Ref. 4 with the important exception of the orientation of $\mathbf{B}_0$. A similar geometry for MRFM was first proposed by Marohn *et al.*[12] in 1998, in order to avoid magnetic spring effects and magnetic dissipation. Our apparatus, however, has the additional advantage of being compatible with the microwire rf sources and patterned magnetic tips designed for nanoscale MRFM.

The cantilever used in this experiment is 150-μm-long, 4-μm-wide, and 0.1-μm-thick and includes a 1-μm-thick mass on its end.[13] A droplet of polystyrene solution is affixed and cured onto the end of the cantilever resulting in a 2-μm-sized particle.[14] The sample-loaded cantilever has a mechanical resonance frequency $\omega_m = 2\pi \times 2.6$ kHz and an intrinsic quality factor $Q = 5.0 \times 10^4$ at $T = 500$ mK. Through measurements of the cantilever's thermal motion, we determine its effective spring constant to be $k = 120$ μN/m. The microwire rf source and nanosized magnetic tip are fabricated in a process similar to that described in Ref. 4. The Au wire is 2.6-μm-long, 1.0-μm-wide, and 0.2-μm-thick and is patterned atop a Si substrate. The FeCo tip deposited atop the microwire is 250 nm tall in the shape of a truncated cone with a diameter at the top and bottom being 270 nm and 510 nm, respectively. The MRFM apparatus is isolated from vibrations and mounted in a vacuum chamber with a pressure below 10^{-6} mbar at the bottom of a continuous flow ^{3}He cryostat. The motion of the lever is detected using 100 nW of 1550 nm laser light focused onto a 10-μm-wide paddle and

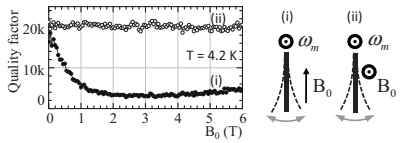

FIG. 1. A nominally nonmagnetic 120 μm × 4 μm × 0.1 μm Si cantilever (Ref. 13). Quality factor Q plotted as a function of magnetic field pointing perpendicular (i) and parallel (ii) to the lever's angular rotation vector.

a)Electronic mail: martino.poggio@unibas.ch.

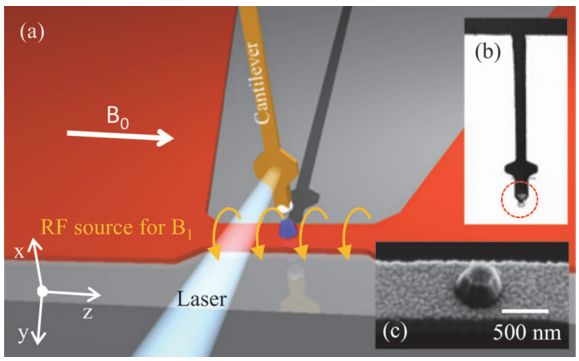

FIG. 2. (Color) (a) Experimental apparatus. Current flows in the microwire (red) along $\hat{z}$ while the lever displacement is along $\hat{y}$. Inset (b) shows an SEM image of a Si cantilever with a polystyrene sample, and (c) shows a SEM of a microwire rf source with an integrated FeCo tip.

reflected back into an optical fiber interferometer.[15] We damp the cantilever to a quality factor of $Q \approx 400$ in order to increase the bandwidth of our force detection without sacrificing force sensitivity.[16]

We measure the statistical polarization of ^{1}H at $T = 500$ mK in the polystyrene particle using the adiabatic rapid passage technique described in Refs. 4 and 14. Experiments are performed with $B_0 > 2.5$ T such that the FeCo tip is fully magnetized along $\hat{z}$. At these fields, the cantilever experiences no magnetic dissipation and maintains its intrinsic Q of 5.0×10^4 far from the microwire surface. During the measurement, the sample at the end of the cantilever is positioned within 200 nm of the FeCo tip. Upon such close approach to the FeCo tip and microwire, interactions between the sample and the microwire surface begin to dominate the mechanical dissipation;[17] these effects reduce the cantilever Q to 1.5×10^4. While this kind of dissipation can be minimized by using the appropriate coating on the end of the cantilever tip, it remains an important limit on MRFM sensitivity.

Magnetic resonance measurements performed with the sample positioned 150 nm above the FeCo tip are shown in Fig. 3(a). The line shape of the magnetic resonance signal as a function of rf carrier frequency is seen to change as the sample is moved from being directly above the FeCo tip along $\hat{z}$ in steps of 240 nm. A similar experiment, in which the sample is positioned to one side of the FeCo tip, such that

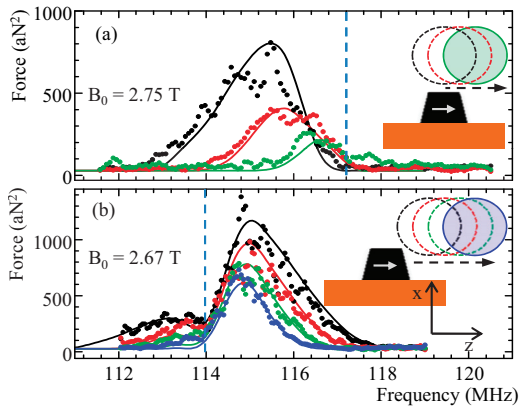

FIG. 3. (Color) ^{1}H spin signal in a polystyrene sample as a function of rf carrier frequency. Points are experimental data while solid lines are simulations. The insets depict the positions of the sample (colored circles) for each resonance curve relative to the FeCo tip (magnetized along the white arrow). The dashed lines mark the resonance frequencies of ^{1}H spins at B_0.

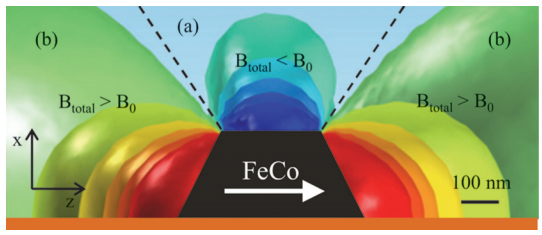

FIG. 4. (Color) Cross section through the center of the FeCo tip with resonant slices in the xz-plane (surfaces of constant B_{total}). White arrow shows the magnetization direction of FeCo.

its surface is about 80 nm from the closest point on the FeCo tip, is shown in Fig. 3(b). Here the magnetic resonance line shape changes as the sample is moved away from the FeCo tip along $\hat{z}$ in steps of 60 nm. The data, shown as points, demonstrate a narrowing of resonance line as the sample moves away from the FeCo tip indicating gradients exceeding 10^5 T/m within a 100 nm spacing.[18]

In order to extract more detailed information from these resonances, a simple theory is constructed from a magnetostatic model of the FeCo tip and an effective field model for adiabatic rapid passage in the manner of the appendix in Ref. 2. The model's input parameters include the geometry of the FeCo tip and sample taken from scanning electron microscope (SEM) images, the mechanical characteristics of the cantilever, and the form of the adiabatic sweeps.[14] Using realistic parameters, we see a good agreement between our model and the data, especially considering our approximate knowledge of the morphology of the sample. The drop-like sample is modeled as a sphere with a radius of 625 nm, close to the radius of curvature observed by SEM. This agreement allows us to plot the likely field distribution around the FeCo tip in Fig. 4. In this figure, we show the surfaces of constant field around the FeCo tip for a saturating field $\mathbf{B}_0$ pointing along $\hat{z}$. In MRFM, these regions are also known as "resonant slices" since they describe the region in space occupied by the spins resonant with a particular carrier frequency ω_{rf}. ω_{rf} is determined by the magnetic resonance condition $\omega_{\text{rf}}/\gamma = B_{\text{total}} = |\mathbf{B}_0 + \mathbf{B}_{\text{tip}}|$, where γ is the gyromagnetic ratio of the isotope of interest, and $\mathbf{B}_{\text{tip}}$ is the field provided by the FeCo magnet. The form and position of a resonant slice determines the point-spread function of an MRFM measurement and thus is required for any imaging application.[2]

In Fig. 4, we see that there are two types of resonant slice regions; (a) where $B_{\text{total}} < B_0$ and (b) where $B_{\text{total}} > B_0$. The experiments shown in Fig. 2, show that strong signal can be observed both when the sample is in region (a) as in Fig. 3(a) and when the sample is in region (b) as in Fig. 3(b). Note that the resonance signal in Fig. 3(a) appears at carrier frequencies lower than the magnetic resonance condition at B_0 (represented by the dashed line). This result depends on the fact that during this experiment the sample is always within region (a). Thus $B_{\text{total}} < B_0$ for all spins in the sample, resulting in magnetic resonance only for frequencies less than the B_0 resonance. Likewise, for a sample always in region (b), such as shown in Fig. 3(b), resonant signal appears only for frequencies greater than the B_0 resonance. Note that the small amount of signal observed for frequencies greater (less) than the B_0 resonance in Fig. 3(a) [Fig. 3(b)] results from the small parts of the sample that protrude into the adjacent region. In both cases, as expected, the amplitude of

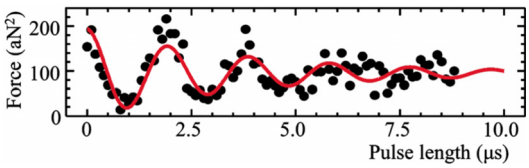

FIG. 5. (Color online) Spin nutation at $T=400$ mK. Force signal is measured as a function of pulse length. A B_1 of 12 mT is extracted from a decaying sinusoidal fit of the Rabi oscillations shown in red.

the spin signal increases as the sample moves closer to the FeCo tip, where magnetic field gradients are stronger. Using the magnetostatic model of Fig. 4 we can extrapolate that in both regions (a) and (b), the maximum gradient relevant to MRFM ($\partial B_{\text{total}}/\partial y$) exceeds 10^6 T/m within 50 nm of the FeCo tip. More precise bounds on this gradient cannot be given because of the approximate model of the morphology of the sample. While gradients in region (a) are always smaller than in region (b) for similar spacings, both are comparable to gradients reported in the most recent realizations of nanoscale MRFM.

These experiments demonstrate that MRFM can be done both with a sample positioned in the region above and in the region next to the FeCo tip. Importantly, the positioning of the sample mounted on the end of the cantilever next to the FeCo tip does not cause the cantilever to snap in to contact even for spacings down to 50 nm. The problem of snap in, which is typically due to electrostatic and van der Waals forces, is avoided here because while the cantilever is extremely soft along $\hat{y}$, it is stiff along $\hat{z}$, and extremely stiff along $\hat{x}$.

The accessibility of the different resonant slice regions depicted in Fig. 4 allows for additional flexibility in future nano-MRI imaging experiments. The shape of the resonant slices and the distribution of the magnetic field gradients determines the point spread function for imaging and therefore the resolution of the technique in each spatial direction. In region (a), for instance, strong gradients in $\hat{x}$ provide high spatial resolution along this direction while smaller gradients in the yz-plane reduce the resolution in those directions. Region (b), on the other hand, offers large gradients and high resolution in $\hat{z}$ and reduced gradients and resolution in the xy-plane. The most recent high resolution imaging experiments have positioned the sample directly above the FeCo tip, achieving high spatial resolution in one direction and reduced resolution in the remaining two. By using the additional region next to the FeCo tip, the high spatial resolution could also be achieved in one more direction, allowing for a more complete high resolution image.

In order to measure the magnitude of B_1 we apply the spin nutation waveform described in Refs. 4 and 14 to our microwire source. Pulses of variable length are inserted in the adiabatic sweep waveform every 500 cantilever cycles (190 ms), resulting in the spin nutation signal shown in Fig. 5. By fitting the data to a decaying sinusoid, we can infer that the rotating rf magnetic field B_1 exceeds 12 mT (510 kHz for ^{1}H) within 200 nm of the magnetic tip for $T<500$ mK. The correlation time τ_m of the spin signal was estimated from the signal bandwidth and found to be on the order of 500 ms. This value is significantly longer than the ~20 ms observed for ^{1}H in previous experiments on organic material,[2] possibly due to the three times larger B_1 applied here.[4] Such a long τ_m allows for the use of pulse protocols that can improve the signal-to-noise ratio and therefore the imaging resolution of nanoscale MRFM.[5] The generation of large B_1 fields is also an important technical achievement since MRFM protocols utilizing adiabatic rapid passage must satisfy the adiabatic limit $(\gamma B_1)^2 \gg \omega_m \Omega_{\text{rf}}$ in order to produce a signal. Here Ω_{rf} is the frequency modulation amplitude of the adiabatic sweep waveform. Nuclear species with low γ therefore require a large B_1 in order to be observable by MRFM. In addition, nuclear resonances broadened by strain or other effects require large Ω_{rf}. Therefore, this large measured B_1 amplitude indicates that nuclear MRFM on previously inaccessible samples such as In or As nuclei in single self-assembled InAs QDs, could be possible.

Assuming a magnetic field gradient of greater than 10^6 T/m within 50 nm of our FeCo tip, and the low temperature force noise of our cantilever near the surface of less than 10 aN/$\sqrt{\text{Hz}}$, we estimate that our technique has a minimum detectable moment of 1.0×10^{-23} J T^{-1} Hz$^{-1/2}$ at this distance. For In moments in InAs self-assembled QDs, for example, this value represents a sensitivity to the statistical polarization of an ensemble of 1.6×10^4 In moments in a typical integration time of one minute.[2] Given that there are between 10^4 and 10^5 In nuclei in a typical self-assembled QD, these parameters promise that imaging of single QDs by MRFM should be possible.

Data shown in Fig. 1 were taken in Dr. Dan Rugar's laboratory at IBM Almaden. We acknowledge support from the Canton Aargau, the Swiss NSF (Grant No. 200021 1243894), and the Swiss Nanoscience Institute.

[1]M. Poggio and C. L. Degen, Nanotechnology **21**, 342001 (2010).
[2]C. L. Degen, M. Poggio, H. J. Mamin, C. T. Rettner, and D. Rugar, Proc. Natl. Acad. Sci. U.S.A. **106**, 1313 (2009).
[3]H. J. Mamin, T. H. Oosterkamp, M. Poggio, C. L. Degen, C. T. Rettner, and D. Rugar, Nano Lett. **9**, 3020 (2009).
[4]M. Poggio, C. L. Degen, C. T. Rettner, H. J. Mamin, and D. Rugar, Appl. Phys. Lett. **90**, 263111 (2007).
[5]C. L. Degen, M. Poggio, H. J. Mamin, and D. Rugar, Phys. Rev. Lett. **99**, 250601 (2007).
[6]T. D. Stowe, K. Yasumura, T. W. Kenny, D. Botkin, K. Wago, and D. Rugar, Appl. Phys. Lett. **71**, 288 (1997).
[7]B. C. Stipe, H. J. Mamin, T. D. Stowe, T. W. Kenny, and D. Rugar, Phys. Rev. Lett. **86**, 2874 (2001).
[8]J. G. E. Harris, R. Knobel, K. D. Maranowski, A. C. Gossard, N. Samarth, and D. D. Awschalom, Appl. Phys. Lett. **82**, 3532 (2003).
[9]D. A. Harrington, P. Mohanty, and M. L. Roukes, Physica B **284–288**, 2145 (2000).
[10]P. Mohanty, D. A. Harrington, K. L. Ekinci, Y. T. Yang, M. J. Murphy, and M. L. Roukes, Phys. Rev. B **66**, 085416 (2002).
[11]T. N. Ng, N. E. Jenkins, and J. A. Marohn, IEEE Trans. Magn. **42**, 378 (2006).
[12]J. A. Marohn, R. Fainchtein, and D. D. Smith, Appl. Phys. Lett. **73**, 3778 (1998).
[13]B. W. Chui, Y. Hishinuma, R. Budakian, H. J. Mamin, T. W. Kenny, and D. Rugar, *Transducers: The 12th International Conference on Solid-State Sensors, Actuators, and Microsystems* (IEEE, Piscataway, NJ, 2003), Vol. 2, p. 1120.
[14]See supplementary material at http://dx.doi.org/10.1063/1.3579521 for more details on the experiments.
[15]D. Rugar, H. J. Mamin, and P. Guethner, Appl. Phys. Lett. **55**, 2588 (1989).
[16]J. L. Garbini, K. J. Bruland, W. M. Dougherty, and J. A. Sidles, J. Appl. Phys. **80**, 1951 (1996); K. J. Bruland, J. L. Garbini, W. M. Dougherty, and J. A. Sidles, *ibid.* **80**, 1959 (1996).
[17]B. C. Stipe, H. J. Mamin, T. D. Stowe, T. W. Kenny, and D. Rugar, Phys. Rev. Lett. **87**, 096801 (2001); S. Kuehn, R. F. Loring, and J. A. Marohn, *ibid.* **96**, 156103 (2006).
[18]E. Nazaretski, E. A. Akhadov, I. Martin, D. V. Pelekhov, P. C. Hammel, and R. Movshovich, Appl. Phys. Lett. **92**, 214104 (2008).